Supporting Information

Wang et al. 10.1073/pnas.1210923109

SI Text

Structural and Circuit Design of a Gyrotropic Unit Cell. The gyrotropic metamaterial featured in this paper is designed in a two-step process to produce a strong Faraday rotation (Fig. S1). In the first step, we introduce directionality (i.e., nonreciprocal transmission) by using one-way circuit elements (unit-gain linear amplifiers) that link a pair of input antennas with a pair of output antennas. The circuit layout restricts the signal flow to a prescribed direction. The second step involves creating a nonreciprocal rotation of the polarization angle with two different assemblies of windmill structures: one with clockwise chirality and the other, counterclockwise. Not only is the chirality opposite, the prescribed signal flows of the two different assemblies (white arrows in Fig. S1) are chosen to be antiparallel. In addition, the orientation of the input antennas is orthogonal to the orientation of the output antennas. When waves travel through the metamaterial along different directions, the polarization of the transmitted waves is modified by the orientation of the output antennas, which are arranged in such a way that the change of polarization angle is opposite for the forward and the backward directions. The windmill structure further allows two orthogonal linear polarizations in the incident wave to be rotated by the same amount. Thus, as a metamaterial, this structure exhibits the Faraday rotation for arbitrarily polarized incident waves.

The operational principle of the metamaterial can be understood by tracing the signal flow in a primitive cell consisting of one set of two neighboring assemblies, as illustrated in Fig. S2. Because any coherent wave can be decomposed into two orthogonal linearly polarized components, these components can be considered separately.

Taking the vertically polarized front-side incidence as an example (Fig. S2, *Top*), one needs to consider three paths of signal flow. The top path is mediated through the top assembly (red): The vertical dipole antennas on the front board absorb part of the incident power, and drive the amplifier mounted at the center. Here, a small gain is set to compensate the total loss of the antenna system without causing self-excitation. The recovered signals subsequently emit through the horizontal dipole antennas on the back board. The emitted wave is now horizontally polarized with an amplitude of $A_1 e^{i\phi}$, where ϕ is the phase shift introduced by the antenna-amplifier system. Similarly, the bottom path is mediated through the lower assembly (orange), and a phase delay of ϕ is incurred through the antenna-amplifier system. However, an additional phase delay, $2\theta = 2k_0 d$, is also incurred. Here, k_0 denotes the propagation constant in free space, and d denotes the effective thickness of the metamaterial. Because of the symmetry of the structure, the transmitted wave along this path carries the same power as the one along the top path, and its amplitude takes the form of $A_1 e^{i(\phi+2\theta)}$. Therefore, the total amplitude of the horizontally polarized transmitted wave is $A_1 e^{i(\phi+2\theta)} + A_1 e^{i\phi} = 2A_1 \cos\theta e^{i(\phi+\theta)}$. As the third path, the remaining power of the incident wave travels through the structure without interacting with either assembly. After traversing the metamaterial, this wave remains vertically polarized, with a phase shift of $\theta = k_0 d$. The amplitude of such a wave is $A_2 e^{i\theta}$. Apparently, in order to accomplish linearly polarized output, one needs to adjust the phase response of the amplifiers such that ϕ vanishes or is equal to π. In doing so, the overall output wave is maintained to be linearly polarized, but with a rotated polarized angle ($\Delta\varphi = \arctan\frac{2A_1\cos\theta}{A_2}$). Because of the fourfold rotational symmetry along the optical axis, horizontally polarized incident waves—and, more generally, incident waves linearly polarized at an arbitrarily angle—experience an identical rotation in the polarization angle.

For waves incident from the back side, we can similarly track the phase changes incurred through all three paths (Fig. S2*B*). The direct path again yields a transmitted wave with an amplitude of $A_2 e^{i\theta}$. However, transmitted waves mediated through the two assemblies now incur phase shifts of $\phi + \pi$ and $\phi + 2\theta + \pi$, respectively. The amplitude of such a horizontally polarized wave is therefore $-2A_1 \cos\theta e^{i(\phi+\theta)}$, resulting in a rotation in the polarization angle of the overall transmitted wave to be $-\Delta\varphi$. Such a negative sign for the backward propagation is the hallmark of the Faraday rotation, indicating that the metamaterial behaves as a gyrotropic medium.

Characterization of the Polarization State. In order to verify the Faraday rotation of the gyrotropic metamaterial, one needs to confirm that the transmitted wave is linear-polarized and that the change of polarization angle is nonreciprocal. For this purpose, the full polarization state of the transmitted signal is characterized through power and polarization patterns in numerical simulations.

At any given frequency, for incident waves with the E fields polarized along x direction $E_{i,x} = a_0$, the transmitted waves are completely described by $E_{o,x} = a_x e^{ip_x}$ and $E_{o,y} = a_y e^{ip_y}$, where both $a_{x(y,0)}$ and $p_{x(y)}$ are real-valued quantities.

The power pattern of the transmitted waves as a function of angle θ is defined as

$$S(\theta) = \frac{1}{a_0^2}|a_x e^{ip_x}\cos\theta + a_y e^{ip_y}\sin\theta|^2,$$

which can be directly measured by the scalar network analyzer.

The polarization pattern of the transmitted waves as a function of angle θ is obtained by sweeping ψ from 0 to 2π, and through the following quantities (1):

$$A(\psi) = a_x\cos(p_x - \psi),\ B(\psi) = a_y\cos(p_y - \psi)$$

The polarization amplitude is defined as

$$\rho(\psi) = [a_x^2\cos^2(p_x - \psi) + a_y^2\cos^2(p_y - \psi)]^{0.5}$$

The polar angle θ is related to ψ as

$$\theta = \begin{cases} \arcsin\frac{B(\psi)}{\rho(\psi)} & \text{for} A(\psi) \geq 0 \\ \pi - \arcsin\frac{B(\psi)}{\rho(\psi)} & \text{for} A(\psi) < 0 \end{cases}.$$

Constitutive Parameters of the Gyrotropic Medium. ***Eigenstates (Normal Modes in Gyrotropic Media).*** At frequency ω_0, we consider a gyrotropic medium with the following permittivity and permeability properties:

$$\bar{\bar{\varepsilon}} = \varepsilon_0\begin{bmatrix} \varepsilon_r & -i\varepsilon_g & 0 \\ i\varepsilon_g & \varepsilon_r & 0 \\ 0 & 0 & \varepsilon_{rz} \end{bmatrix},$$

$$\bar{\bar{\mu}} = \mu_0\begin{bmatrix} \mu_r & 0 & 0 \\ 0 & \mu_r & 0 \\ 0 & 0 & \mu_{rz} \end{bmatrix},$$

where a dc magnetic field is applied in $\hat{z}$ direction. An anisotropic medium characterized by such hermitian permittivity tensor is called gyroelectric or electrically gyrotropic (1).

Inside this gyrotropic medium, the eigenmodes of the electromagnetic plane waves propagating in $-\hat{z}$ direction are two circularly polarized modes: $E_0(\hat{x}+i\hat{y})$ and $E_0(\hat{x}-i\hat{y})$. A linearly polarized plane wave can be decomposed into:

$$\begin{aligned}\overline{D} &= \frac{D_0}{2}(\hat{x}+i\hat{y})e^{i\phi_{+i}} + \frac{D_0}{2}(\hat{x}-i\hat{y})e^{i\phi_{-i}} \\ &= \hat{x}\frac{D_0}{2}(e^{i\phi_{+i}}+e^{i\phi_{-i}}) + i\hat{y}\frac{D_0}{2}(e^{i\phi_{+i}}-e^{i\phi_{-i}}).\end{aligned}$$

Because of the circular birefringence induced by the dc magnetic field, there is a difference between the single-pass phase shifts ϕ_{+i} and ϕ_{-i}, which result in the following Faraday rotation:

$$\frac{D_y}{D_x} = i\frac{e^{i\phi_{+i}}-e^{i\phi_{-i}}}{e^{i\phi_{+i}}+e^{i\phi_{-i}}} = -\tan\frac{\phi_{+i}-\phi_{-i}}{2}.$$

Looking through $-\hat{z}$ direction, rotation angle θ (see Fig. S3) is equal to $\frac{\phi_{-i}-\phi_{+i}}{2}$.

This difference between ϕ_{+i} and ϕ_{-i} is a direct consequence of the two eigenmodes having different phase velocity in a gyrotropic medium:

$$\begin{cases}\phi_{+i} = \frac{\omega_0 L}{c}\sqrt{\mu_r(\varepsilon_r+\varepsilon_g)} \\ \phi_{-i} = \frac{\omega_0 L}{c}\sqrt{\mu_r(\varepsilon_r-\varepsilon_g)}\end{cases}.$$

Reflection and transmission coefficients. See Fig. S4. For plane waves traveling along $\hat{z}$ we can write down the wave impedance for the eigenmodes both inside and outside the gyrotropic medium:

$$\eta_{1,+i} = \eta_{1,-i} = \eta_1 = \sqrt{\mu_0/\varepsilon_0}, \qquad \eta_{2,+i} = \eta_1\sqrt{\mu_r/(\varepsilon_r+\varepsilon_g)},$$
$$\eta_{2,-i} = \eta_1\sqrt{\mu_r/(\varepsilon_r-\varepsilon_g)}.$$

Taking into account the Fresnel reflection and transmission at the two interfaces,

$$\begin{aligned}R_{12,+i} &= \frac{\eta_{2,+i}-\eta_1}{\eta_{2,+i}+\eta_1}, & R_{21,+i} &= \frac{\eta_1-\eta_{2,+i}}{\eta_{2,+i}+\eta_1}, \\ T_{12,+i} &= \frac{2\eta_{2,+i}}{\eta_{2,+i}+\eta_1}, & T_{21,+i} &= \frac{2\eta_1}{\eta_{2,+i}+\eta_1}, \\ R_{12,-i} &= \frac{\eta_{2,-i}-\eta_1}{\eta_{2,-i}+\eta_1}, & R_{21,-i} &= \frac{\eta_1-\eta_{2,-i}}{\eta_{2,-i}+\eta_1}, \\ T_{12,-i} &= \frac{2\eta_{2,-i}}{\eta_{2,-i}+\eta_1}, & T_{21,-i} &= \frac{2\eta_1}{\eta_{2,-i}+\eta_1},\end{aligned}$$

we can derive the transmitted and the reflected waves for any incident polarization. Consider an incident wave with the electric field polarized in the $\hat{x}$ direction, $E_i = \hat{x}E_0$, we find both x and y components of the reflected wave and transmitted waves at the slab surface:

$$\begin{aligned}T_{+i} &= \frac{E_0}{2}(\hat{x}+i\hat{y})[T_{12,+i}T_{21,+i}e^{i\phi_{+i}} \\ &\quad + T_{12,+i}T_{21,+i}e^{i\phi_{+i}}(R_{21,+i}^2e^{2i\phi_{+i}}) \\ &\quad + T_{12,+i}T_{21,+i}e^{i\phi_{+i}}(R_{21,+i}^2e^{2i\phi_{+i}})^2 + \ldots] \\ &= \frac{E_0}{2}(\hat{x}+i\hat{y})T_{12,+i}T_{21,+i}e^{i\phi_{+i}}\sum_{n=0}^{\infty}(R_{21,+i}^2e^{2i\phi_{+i}})^n \\ &= \frac{E_0}{2}(\hat{x}+i\hat{y})T_{12,+i}T_{21,+i}e^{i\phi_{+i}}\frac{1}{1-R_{21,+i}^2e^{2i\phi_{+i}}},\end{aligned}$$

$$\begin{aligned}T_{-i} &= \frac{E_0}{2}(\hat{x}-i\hat{y})[T_{12,-i}T_{21,-i}e^{i\phi_{-i}} + T_{12,-i}T_{21,-i}e^{i\phi_{-i}}(R_{21,-i}^2e^{2i\phi_{-i}}) \\ &\quad + T_{12,-i}T_{21,-i}e^{i\phi_{-i}}(R_{21,-i}^2e^{2i\phi_{-i}})^2 + \ldots.] \\ &= \frac{E_0}{2}(\hat{x}-i\hat{y})T_{12,-i}T_{21,-i}e^{i\phi_{-i}}\sum_{n=0}^{\infty}(R_{21,-i}^2e^{2i\phi_{-i}})^n \\ &= \frac{E_0}{2}(\hat{x}-i\hat{y})T_{12,-i}T_{21,-i}e^{i\phi_{-i}}\frac{1}{1-R_{21,-i}^2e^{2i\phi_{-i}}}\end{aligned}$$

$$\begin{aligned}R_{+i} &= \frac{E_0}{2}(\hat{x}+i\hat{y})[R_{12,+i}+T_{12,+i}T_{21,+i}R_{21,+i}e^{2i\phi_{+i}} \\ &\quad + T_{12,+i}T_{21,+i}R_{21,+i}e^{2i\phi_{+i}}(R_{21,+i}^2e^{2i\phi_{+i}}) \\ &\quad + T_{12,+i}T_{21,+i}R_{21,+i}e^{2i\phi_{+i}}(R_{21,+i}^2e^{2i\phi_{+i}})^2 + \ldots] \\ &= \frac{E_0}{2}(\hat{x}+i\hat{y})[R_{12,+i}+T_{12,+i}T_{21,+i}R_{21,+i}e^{2i\phi_{+i}}\sum_{n=0}^{\infty}(R_{21,+i}^2e^{2i\phi_{+i}})^n] \\ &= \frac{E_0}{2}(\hat{x}+i\hat{y})\left[R_{12,+i}+T_{12,+i}T_{21,+i}R_{21,+i}e^{2i\phi_{+i}}\frac{1}{1-R_{21,+i}^2e^{2i\phi_{+i}}}\right],\end{aligned}$$

$$\begin{aligned}R_{-i} &= \frac{E_0}{2}(\hat{x}-i\hat{y})[R_{12,-i}+T_{12,-i}T_{21,-i}R_{21,-i}e^{2i\phi_{-i}} \\ &\quad + T_{12,-i}T_{21,-i}R_{21,-i}e^{2i\phi_{-i}}(R_{21,-i}^2e^{2i\phi_{-i}}) \\ &\quad + T_{12,-i}T_{21,-i}R_{21,-i}e^{2i\phi_{-i}}(R_{21,-i}^2e^{2i\phi_{-i}})^2 + \ldots] \\ &= \frac{E_0}{2}(\hat{x}-i\hat{y})[R_{12,-i}+T_{12,-i}T_{21,-i}R_{21,-i}e^{2i\phi_{-i}}\sum_{n=0}^{\infty}(R_{21,-i}^2e^{2i\phi_{-i}})^n] \\ &= \frac{E_0}{2}(\hat{x}-i\hat{y})\left[R_{12,-i}+T_{12,-i}T_{21,-i}R_{21,-i}e^{2i\phi_{-i}}\frac{1}{1-R_{21,-i}^2e^{2i\phi_{-i}}}\right].\end{aligned}$$

Here, we have used the following single-pass phase shift, as derived in *Section 3.1*:

$$\begin{cases}\phi_{+i} = \frac{\omega_0 L}{c}\sqrt{\mu_r(\varepsilon_r+\varepsilon_g)} \\ \phi_{-i} = \frac{\omega_0 L}{c}\sqrt{\mu_r(\varepsilon_r-\varepsilon_g)}\end{cases}.$$

Optimized constitutive parameters from simulated S-parameters. The Computer Simulation Technology (CST) model provides us with four ports: port1 (front, h), port2 (front, v), port3 (back, h), port4 (back, v), all linearly polarized (see Fig. S5). Assuming that all four ports are at the same distance, D, away from the surfaces of the gyrotropic slab and the system is excited by port1, we can convert the simulated S-matrix element into effective permittivity and permeability tensor elements of the gyrotropic medium:

$$S_{31} = T_x e^{2ik_0 D}/E_0$$
$$= e^{2ik_0 D}\frac{1}{2}\left[T_{12,+i}T_{21,+i}e^{i\phi_{+i}}\frac{1}{1-R_{21,+i}^2 e^{2i\phi_{+i}}} + T_{12,-i}T_{21,-i}e^{i\phi_{-i}}\frac{1}{1-R_{21,-i}^2 e^{2i\phi_{-i}}}\right],$$
$$S_{41} = T_y e^{2ik_0 D}/E_0$$
$$= e^{2ik_0 D}\frac{1}{2}i\left[T_{12,+i}T_{21,+i}e^{i\phi_{+i}}\frac{1}{1-R_{21,+i}^2 e^{2i\phi_{+i}}} - T_{12,-i}T_{21,-i}e^{i\phi_{-i}}\frac{1}{1-R_{21,-i}^2 e^{2i\phi_{-i}}}\right],$$
$$S_{11} = R_x e^{2ik_0 D}/E_0$$
$$= e^{2ik_0 D}\frac{1}{2}\left[R_{12,+i} + T_{12,+i}T_{21,+i}R_{21,+i}e^{2i\phi_{+i}}\frac{1}{1-R_{21,+i}^2 e^{2i\phi_{+i}}} + R_{12,-i} + T_{12,-i}T_{21,-i}R_{21,-i}e^{2i\phi_{-i}}\frac{1}{1-R_{21,-i}^2 e^{2i\phi-i}}\right],$$
$$S_{21} = R_y e^{2ik_0 D}/E_0$$
$$= e^{2ik_0 D}\frac{1}{2}i\left[R_{12,+i} + T_{12,+i}T_{21,+i}R_{21,+i}e^{2i\phi_{+i}}\frac{1}{1-R_{21,+i}^2 e^{2i\phi_{+i}}} - R_{12,-i} - T_{12,-i}T_{21,-i}R_{21,-i}e^{2i\phi_{-i}}\frac{1}{1-R_{21,-i}^2 e^{2i\phi_{-i}}}\right],$$

where $k_0 = \omega_0/c$.

Here the S-matrix, described in Table S1, is clearly asymmetric, and thus the system is nonreciprocal.

In the CST simulation model, the distance between the ports on the front side and the ports on the back side is 0.348 m. The optimized results at 805 MHz are listed in Tables S2 and S3.

The constitutive parameters of this gyrotropic medium are:

$$\bar{\bar{\varepsilon}} = \varepsilon_0\begin{bmatrix} 0.08+i0.14 & -i(0.27+i0.09) & 0 \\ i(0.27+i0.09) & 0.08+i0.14 & 0 \\ 0 & 0 & \varepsilon_{rz}\end{bmatrix},$$

$$\bar{\bar{\mu}} = \mu_0\begin{bmatrix} 0.9+i0.08 & 0 & 0 \\ 0 & 0.9+i0.08 & 0 \\ 0 & 0 & \mu_{rz}\end{bmatrix}.$$

Note tensor elements ε_{rz} and μ_{rz} are inconsequential to the propagation of plane waves traveling along the $\hat{z}$ direction, and do not affect the gyrotropic property of the metamaterial.

The frequency dependence of the constitutive parameters in the operating frequency band are shown in Fig. S6.

1. Kong JA (2008) *Electromagnetic Wave Theory* (EMW, Cambridge) 2008 Ed, Chap 1.2, pp 24–44; Chap 3.1, pp 263–291; Chap 3.2, pp 292–305.

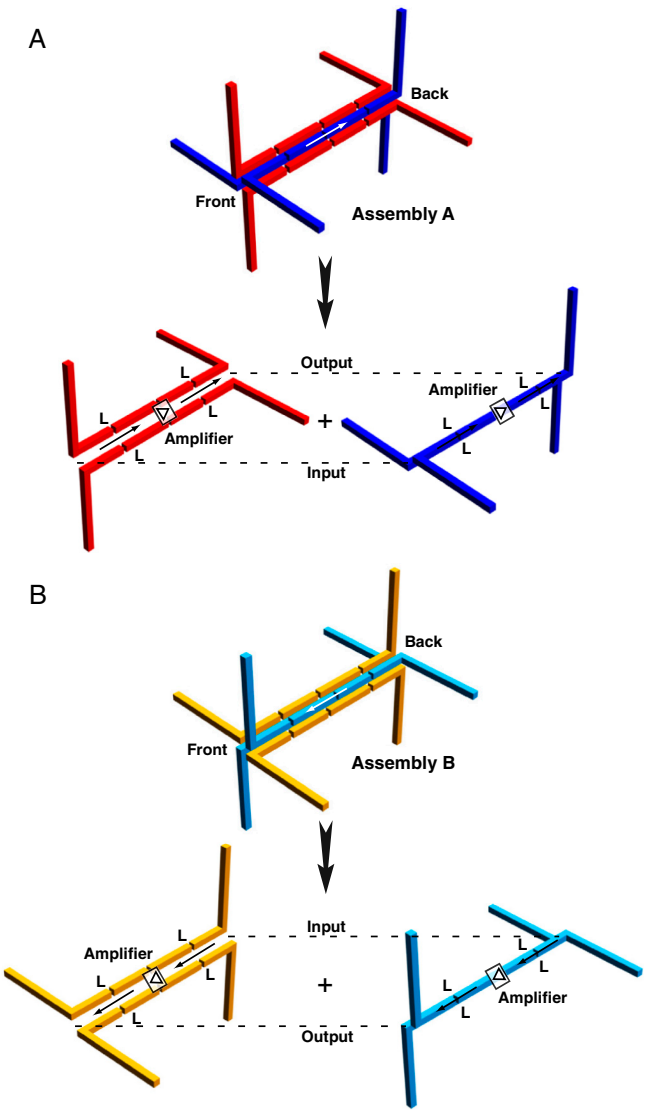

Fig. S1. Decomposition of (*A*) assembly A and (*B*) assembly B, two different types used in the unit cell of the metamaterial. The directionality of the active circuits and the polarization of the input/output antennas are illustrated. L indicates the inductors for impedance matching of the antennas.

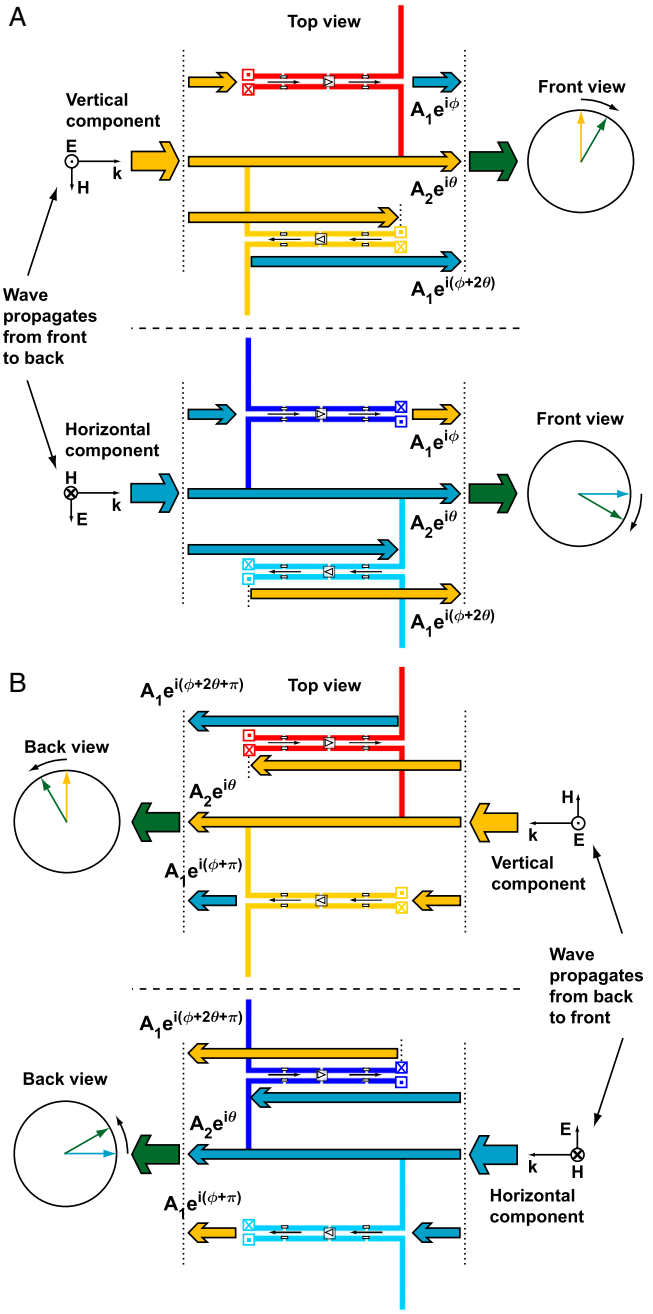

Fig. S2. Signal paths for incident waves of two orthogonal polarizations incident from the opposite directions: (*A*) from the front to the back side, and (*B*) from the back to the front. All structures are shown in top view.

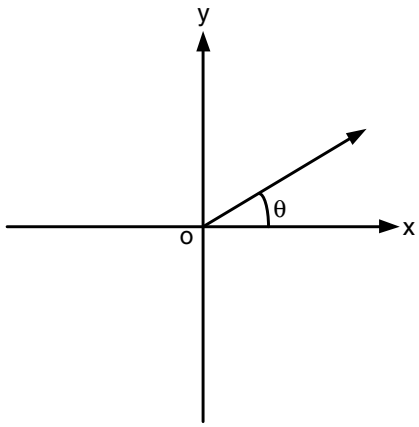

Fig. S3. Definition of the coordinate.

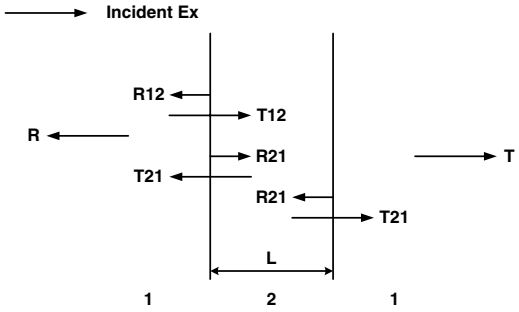

Fig. S4. Diagram of the reflection and transmission of a single-layer medium.

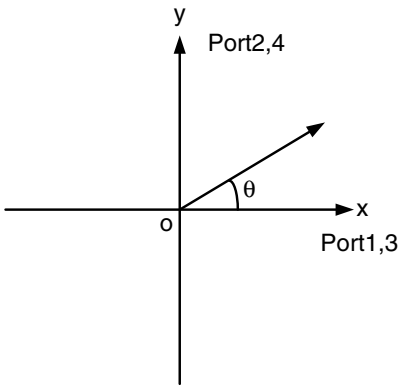

Fig. S5. Port definition of the simulation model.

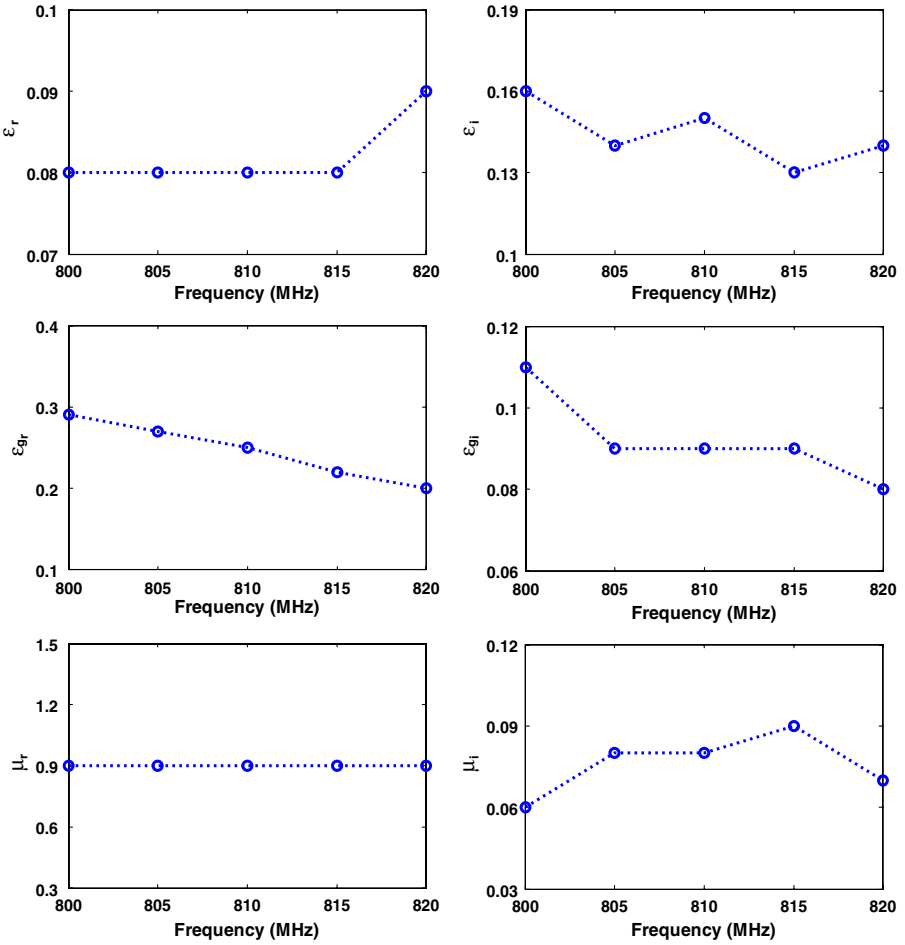

Fig. S6. Frequency dependence of the constitutive parameters.

Table S1. Original data of simulated S-parameters

	S1m	S2m	S3m	S4m
Sn1	$-0.198 - i0.155$	$-0.070 + i0.058$	$0.629 - i0.625$	$-0.064 + i0.055$
Sn2	$0.070 - i0.066$	$-0.194 - i0.153$	$0.064 - i0.063$	$0.634 - i0.621$
Sn3	$0.629 - i0.625$	$-0.064 + i0.055$	$-0.198 - i0.155$	$-0.070 + i0.058$
Sn4	$0.064 - i0.063$	$0.634 - i0.621$	$0.070 - i0.066$	$-0.194 - i0.153$

Table S2. Original data and optimized S-parameters

	S31	S41	S11	S21
Data_Abs	0.8867	0.0844	0.2515	0.0909
Data_Phase	−44.8172	139.3251	−141.9452	140.3558
Op_Abs	0.8882	0.0891	0.2504	0.0852
Op_Phase	−43.8308	140.3177	−140.1495	138.0994

Table S3. Optimized effective thickness of the gyrotropic slab

Op_L	0.04 m	$\mathrm{Op\,D} = (0.348 - \mathrm{Op\,L})/2$	0.154 m